

2012

Biologically-Derived Dye-Sensitized Solar Cells: A Cleaner Alternative for Solar Energy

Erika S. Falsgraf
Pomona College

Recommended Citation

Falsgraf, Erika S., "Biologically-Derived Dye-Sensitized Solar Cells: A Cleaner Alternative for Solar Energy" (2012). *Pomona Senior Theses*. Paper 61.
http://scholarship.claremont.edu/pomona_theses/61

This Open Access Senior Thesis is brought to you for free and open access by the Pomona Student Scholarship at Scholarship @ Claremont. It has been accepted for inclusion in Pomona Senior Theses by an authorized administrator of Scholarship @ Claremont. For more information, please contact scholarship@cuc.claremont.edu.

Biologically-derived dye-sensitized solar cells: A cleaner alternative for solar energy

Erika S. Falsgraf

Thesis prepared for Bachelor of Arts in Environmental Analysis, Chemistry track

2011-2012 academic year, Pomona College, Claremont, CA

Advisor: Malkiat S. Johal

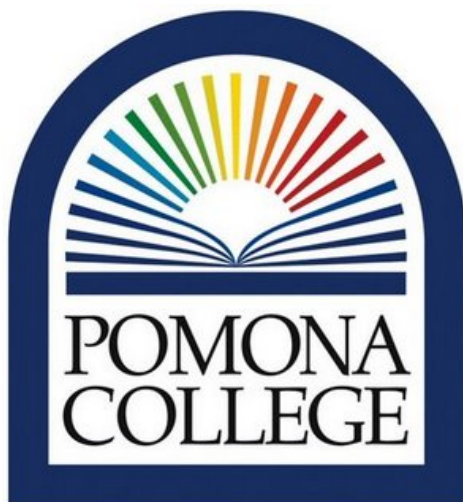


Table of Contents

Abstract	3
1. Introduction	4
1.1 Alternative energy sources.....	4
1.2 Efficiency calculations for photovoltaic cells.....	5
1.3 First and second generation solar cells.....	8
1.4 DSSC overview.....	10
1.5 Dye as a light-harvesting compound.....	12
1.6 Hole transport layer.....	15
1.7 Electron transport layer.....	16
1.8 Experimental design.....	19
2. Experimental	22
2.1 Materials.....	22
2.2 Cell assembly.....	22
2.3 Efficiency characterization.....	25
3. Results and discussion	27
3.1 Scanning electron microscopy.....	27
3.2 UV-visible spectroscopy.....	29
3.3 Voltammetry.....	31
4. Conclusions	38
5. Acknowledgements	39
6. Supplemental data	40
7. References	41

Abstract

This project employs the biological compounds hemin, melanin, and retinoic acid as photoactive dyes in dye-sensitized solar cells (DSSCs). These dyes are environmentally and economically superior to the standard ruthenium-based dyes currently used in DSSCs because they are nontoxic and widely available. Characterization by linear sweep voltammetry yielded averaged maximum overall conversion efficiency values of 0.059% for retinoic acid, 0.023% for melanin, and 0.015% for hemin. Absorption spectra of hemin and retinoic acid suggest that they would complement each other well when used in tandem in one cell because hemin has a secondary maximum absorption peak at 613nm and retinoic acid has maximum absorption at 352nm. Cells made with hemin or melanin performed better with the use of lower temperatures to seal the cells, and hemin cells performed exceptionally well with exclusion of the sealing procedure. These biologically-derived cells have the potential to advance the development of inexpensive and safer solar energy sources, which promise to serve as clean energy sources in the near future.

1. Introduction

1.1 Alternative energy sources

Our current energy consumption predominately relies on fossil fuels that generate greenhouse gases (GHG), most notably carbon dioxide (CO₂). CO₂ emissions have increased at a rate of 1.9% per year over the last three decades and atmospheric CO₂ concentration in 2005 was 379ppm, an increase of almost 100ppm since preindustrial times.¹ GHG are directly implicated in the rise of average global temperatures over the last century, which has widespread effects on ocean levels, biodiversity, crop production, natural disasters, and other aspects of the ecosystem. In addition, the U.S. and other countries depend on foreign fossil fuels, which are often threatened by civil and political unrest, to support their energy demands. Industrialization of developing countries presents serious obstacles for environmental health because poorer economies are more likely to depend on “dirty energy” like coal instead of “clean energy” such as solar or wind power. Furthermore, accelerating population growth implies higher total energy demand regardless of industrialization.

One approach is to decrease energy consumption by changing human habits and developing more efficient appliances, while others support development of energy sources that do not generate harmful byproducts. Photovoltaic (PV) cells fall in the second category of clean energy strategies and hold promise for future generations that do not depend on unreliable and toxic systems of energy production. The Earth receives about 100,000TW of energy from the sun, a fraction

of which could satisfy our current energy demands if we covered 0.1% of Earth's surface with PV cells with efficiencies of 10%. The main obstacle for solar cells today is cost-effectiveness: in 2005, PV energy was five to thirteen times as expensive as wholesale electricity.² This gap must close if solar energy is to be widely accepted because people tend to value inexpensive energy over clean energy. Imminent shortages in fossil fuel production may drive up prices for conventional energy, making alternative energy sources more appealing. However, a more proactive effort to lower solar energy prices would be highly preferable for global economies and ecosystems.

1.2 Efficiency calculations for photovoltaic cells

An understanding of the quantitative evaluation of PVs will be useful for the introduction to solar cells that follows. Assessment of a solar cell's performance involves several parameters, including short-circuit photocurrent density (J_{sc}), open-circuit voltage (V_{oc}), maximum power (P_{max}), fill factor (FF), quantum efficiency (QE) or incident-photon-to-electron conversion efficiency (IPCE), and overall conversion efficiency (η). J_{sc} is the current density generated by a cell during illumination in the absence of a potential difference and V_{oc} is the potential difference developed when there is no current.³ In practice, J_{sc} and V_{oc} are found by using a potentiostat to apply a variable voltage to a cell and calculate the resulting currents generated. This produces a graph of bias voltage vs. current density, with the y-intercept equal to J_{sc} and the x-intercept equal to V_{oc} (Figure 1).

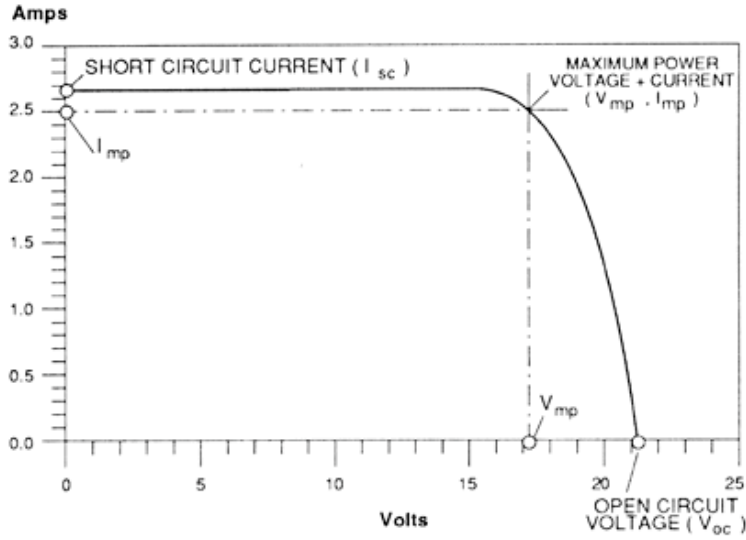


Figure 1. Current-voltage (I-V) curve of a photovoltaic device. Diagram indicates I_{sc} , V_{oc} , and P_{max} . Reproduced from Darling, D.⁴

The cell has a variable power density given by $P = JV$, and it produces maximum power P_{max} at a given J_m and V_m . Fill factor is found by comparing P_{max} to theoretical maximum power, which is given by J_{sc} multiplied by V_{oc} .

$$FF = P_{max} / (J_{sc}V_{oc}) \quad (1)$$

Overall solar-to-electrical energy conversion efficiency is given by the ratio of P_{max} to power of incident radiation (P_{in}).

$$\eta = J_{sc}V_{oc}FF / P_{in} \quad (2)$$

The standard test condition used to illuminate experimental solar cells is an air mass (AM) 1.5 global (G) solar radiation spectrum. AM describes the path length of solar radiation through the atmosphere, and AM 1.5 refers to the path length

when the sun makes a 42° angle with the Earth’s surface. The solar spectrum resembles that of a blackbody at over 5000K and peaks in the visible range because ozone absorbs ultraviolet light and water and CO₂ absorb infrared radiation (Figure 2). The power delivered by the sun per unit area is standardized at 1000 W/m², or 100 mW/cm². This irradiance value differs based on relative positions of the sun and earth, cloud cover, altitude, and morphology of solar cell surfaces.³

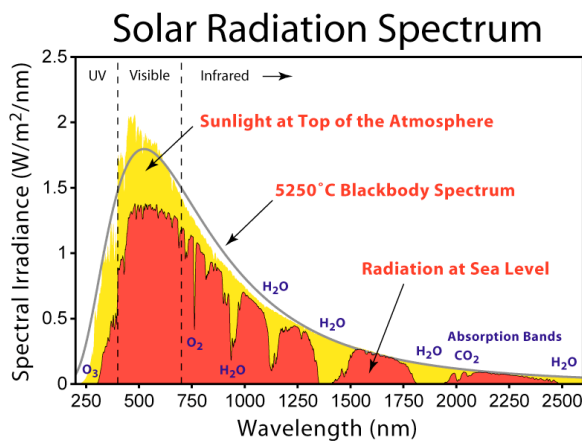


Figure 2. Solar radiation spectrum indicating irradiance at sea level (red fill), at the top of the atmosphere (yellow fill), and a blackbody spectrum (solid line). Reproduced from Rohde, R.A.⁵

The spectral response of a solar cell is described by the IPCE or $QE(\lambda)$ as a function of wavelength. IPCE refers to the probability that an incident photon of wavelength λ will cause one electron to move through the external circuit. By irradiating the cell with chopped monochromatic light while measuring J_{SC} , one can determine the efficiency of photon-to-electron conversion at distinct wavelengths.

IPCE is calculated by

$$IPCE(\lambda) = 124 \cdot J_{SC}(\lambda) / \lambda \cdot P_{in}(\lambda) \quad (3)$$

where λ is the wavelength (nm) at which the monochromator is set, J_{SC} is in units of $\mu\text{A}/\text{cm}^2$, and P_{in} is in units of mW/cm^2 .⁶

When comparing efficiencies, it is important to keep in mind the disparity between commercial modules and laboratory cells. Cells constructed in a lab present higher efficiencies because efforts taken to minimize resistive losses are frequently too expensive to implement in commercial cells. Furthermore, large modules require connections between individual cells which decrease the functional surface area of the module.² High-functioning laboratory cells are the first step in an extensive procedure that results in large-scale modules available for use around the planet.

1.3 First and second generation solar cells

First generation silicon photovoltaic cells are created by doping a silicon semiconductor with materials that have either an excess of electrons (n-doping) or a deficiency of electrons (p-doping). The first silicon solar cell was engineered in 1953 by doping sections of silicon with gallium and lithium, while later models used gallium and phosphorous.⁷ Gallium has three valence electrons and phosphorous has five valence electrons, so excess electrons on the n-layer (phosphorous) flow through the p-n junction to the p-layer (gallium). This generates a positive charge on the n-doped silicon and a negative charge on the p-doped silicon, resulting in an electric field which compels electrons to move from the p-layer to the n-layer under illumination. First generation cells have efficiencies of 12-17% and currently

dominate the market for photovoltaic solar cells with 94% of the market share. However, the industry is facing a shortage of high grade silicon, which has exhibited price increases of \$9 per kilo in 2000 to \$60 per kilo in 2005. This drop in supply means that the price of silicon solar cells will not decrease in the near future, so we must look to other technologies if solar cells are to become economically competitive with fossil fuels.²

Second generation solar cells rely on thin films such as amorphous silicon (a-Si), cadmium telluride (CdTe), and copper indium selenide (CuInSe). Amorphous silicon cells achieve module efficiencies of 5-7% while CdTe and CuInSe cells have achieved module efficiencies of 7-11% and laboratory efficiencies of 15-20%.² Advantages of thin-film cells include ease and low cost of manufacturing, potential for flexible substrates and thus wider range of application, and improved appearance.³ They also have shorter energy pay-back times of about 3 years, compared to 4.5 years for p-n junction cells. However, indium, tellurium, and selenium are relatively scarce, cadmium is a highly toxic heavy metal, and mining of these metals presents various environmental hazards.² Furthermore, cell efficiency is temperature-dependent, which is undesirable for a device meant to be used in full sunlight.³ The environmental and economic drawbacks of first and second generation solar cells demand an inexpensive and environmentally-conscious solar cell.

1.4 DSSC overview

DSSCs exhibit many advantages over previous models of photovoltaic solar cells. Michael Grätzel and Brian O'Regan invented the prototype in 1991, which yielded efficiencies of 7.9%,⁸ and since then development of DSSCs has produced efficiencies as high as 11.1%.² DSSCs contain four major components: a photoactive dye that absorbs light and provides excited electrons, a titanium dioxide (TiO_2) layer that bonds to and receives excited electrons from the dye, a redox electrolyte to transport electrons to the oxidized dye and regenerate initial conditions, and two electrodes to serve as the anode and cathode (Figure 3).⁸ When a photon with sufficient energy strikes the dye, an electron is excited from its ground state in the HOMO (highest occupied molecular orbital) to the LUMO (lowest unoccupied molecular orbital (Figure 4)).⁹ The excited electron is injected into the TiO_2 conduction band, where it travels by diffusion to the anode. The dye is immediately regenerated by the redox electrolyte, typically an iodide/triiodide couple, which reduces the dye so that it may produce another excited electron. The iodide is regenerated at the cathode, which donates electrons to triiodide to reform iodide.¹⁰ The DSSC has defining characteristics of enhanced performance in diffuse light and in environments with high temperatures, low production costs, and potentially higher efficiencies, making it an attractive alternative to p-n junction and thin-film cells.³

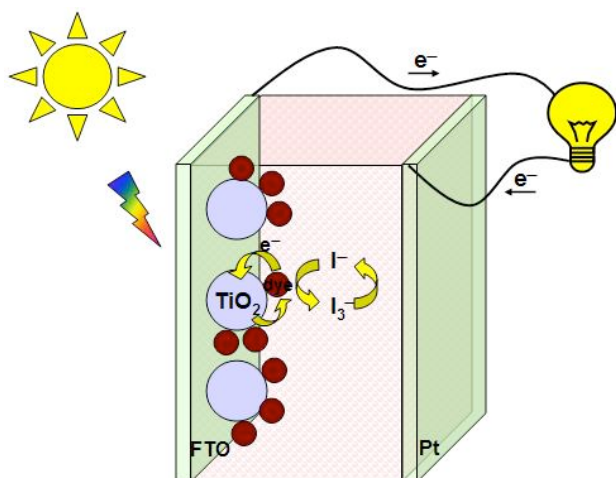


Figure 3. Current generated by a DSSC when exposed to sunlight. Excited electrons from the dye move through a TiO₂ mesoporous structure to the anode while a mobile redox couple (I⁻/I₃⁻) reduces the dye using electrons from the cathode. Reproduced from Sundström, et. al.¹¹

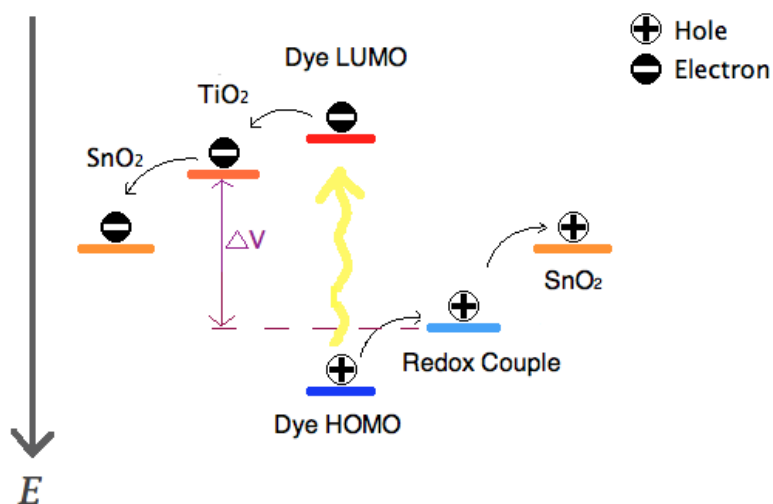


Figure 4. Energy diagram of a DSSC. Electrons are excited from dye HOMO to dye LUMO, inject into the TiO₂ conduction band, and end at the anode. Positive hole left at the dye HOMO are transferred to the redox couple and end at the cathode.

DSSCs perform well in diffuse light because the photoactive dye rests on a mesoporous TiO₂ layer that effectively reflects light toward other dye molecules. P-n junction and thin-film cells suffer significant decreases in efficiency as temperature rises, but DSSC efficiency is nearly independent of temperature in the temperature

range they experience in the real world. DSSCs achieve low production costs by avoiding high-temperature and high-vacuum processes required for silicon cell production and by eliminating the need for silicon as a starting material.² The most expensive component of standard DSSCs is the ruthenium dye, which also happens to be a toxic heavy metal. Ruthenium poses environmental and economic disadvantages to an otherwise elegantly designed solar cell, which serves as inspiration to search for more widely-available and environmentally-friendly dyes.

1.5 Dye as a light-harvesting compound

A photoactive dye is a fundamentally important component of any DSSC because it is responsible for light absorption and electron transfer. The dye, or sensitizer, is essentially a source of excited electrons, which are transported to the anode via the TiO₂ layer. The dye must be small enough to enter the pores in the TiO₂ nanocrystal structure and it must have a functional group that will allow spontaneous assembly by chelating to TiO₂; this is typically a carboxylate group, but phosphonate or hydroxamate groups may also suffice.¹² An ideal dye strongly absorbs radiation across a broad spectrum of wavelengths in the visible range because solar radiation demonstrates maximal output in the visible range (Figure 2). Absorption strength and breadth are determined by a dye's molar absorption coefficient and the HOMO-LUMO energy band gap, respectively, and comparing prototype dyes to ruthenium-based dyes permits evaluation of light absorption characteristics. A dye should be inexpensive and nontoxic if it is to be utilized on a

large scale.⁹ Finally, a marketable DSSC must sustain a turnover number, which refers to the number of electrons transferred from redox electrolyte to dye, of 10^8 in order to last for 15 to 20 years.^{3,13} Efficient dyes that are inexpensive, nontoxic, and resistant to radiation damage will be desirable in commercial DSSCs.

Ruthenium-based organo-metallic complexes have achieved overall conversion efficiencies of greater than 11%. Ruthenium-based complexes exhibit metal-to-ligand charge transfer, a process in which the excited electron in a d-orbital is transferred to the π^* orbital of the carboxyl ligand, from which it is injected into the conduction band of TiO_2 . Molecular engineering has yielded ruthenium compounds with high stabilities, such as dyes N3 and its salt, N719 (Figure 5).¹⁰ The carboxyl moieties on the molecules allow them to chelate to the TiO_2 surface via coordination of the oxide with titanium ions. N3 has absorption maxima at 518 and 380 nm with extinction coefficients of $1.3 \times 10^4 \text{ M}^{-1}\text{cm}^{-1}$ at both wavelengths. It is remarkably stable: N3 in its solid state is stable in air at temperatures up to 280°C and it maintains high performance over 10^8 redox cycles, the equivalent of 15 to 20 years of use.^{3,13} N719 is the deprotonated salt of N3 and demonstrates an enhanced solubility while Z907 is a hydrophobic variant with two long carbon chains; both show absorption across the visible range with little absorption in the near-IR range (Figure 6).

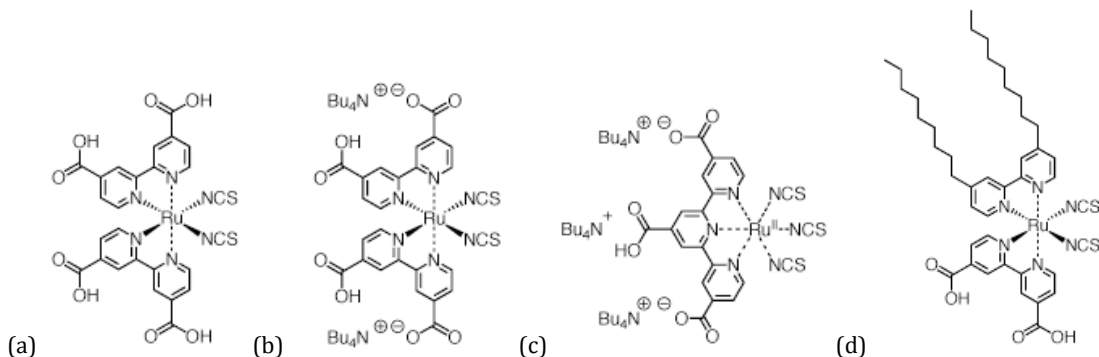


Figure 5. Molecular structures of ruthenium complex dyes: (a) N3, IUPAC name *cis*-bis(isothiocyanato)bis(2,2'-bipyridyl-4,4'-dicarboxylato)-ruthenium(II); (b) N719, IUPAC name *cis*-diisothiocyanato-bis(2,2'-bipyridyl-4,4'-dicarboxylato) ruthenium(II) bis(tetrabutylammonium); (c) Black dye, IUPAC name triisothiocyanato-(2,2':6',6''-terpyridyl-4,4',4''-tricarboxylato) ruthenium(II) tris(tetra-butylammonium); and (d) Z907, IUPAC name *cis*-diisothiocyanato-(2,2'-bipyridyl-4,4'-dicarboxylic acid)-(2,2'-bipyridyl-4,4'-dinonyl) ruthenium(II).

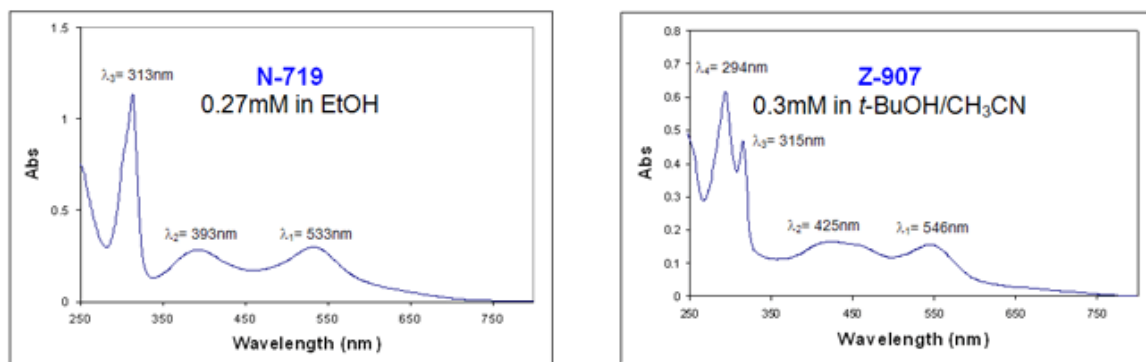


Figure 6. UV/Vis absorption spectra of Ru-based dyes N719 and Z907. Reproduced from Desilvestro & Hebling.¹⁴

Ruthenium-based complexes are the most studied and most efficient dyes developed to date, but the compounds' undesirable features have prompted a search for superior sensitizers. Ruthenium is a rare metal and thus both expensive and environmentally hazardous to mine; the trace amounts that are commercially viable are only found in nickel deposits in South Africa and the Americas. Ruthenium compounds have not been extensively studied for toxicity, but it is recommended that they should be treated as highly toxic and carcinogenic.¹⁵ When heated in the presence of air, they form ruthenium tetroxide, a highly volatile and toxic compound

that damages the eyes and upper respiratory system.¹⁶ Ruthenium-based sensitizers are not feasible for use in mass-produced, sustainable solar cells. This research, therefore, investigates various organic sensitizers to serve as nontoxic and affordable alternatives.

1.6 Hole transport layer

The HTL contains mobile ions that transfer charge from cathode to dye in order to reduce the dye. Ideal HTLs are long-lasting, nontoxic, and can rapidly transport electrons. Solutions using I⁻/I₃⁻ are currently the most popular and efficient hole transporters. Solvents based on organic nitriles (e.g. acetonitrile) yield the highest efficiencies while those based on ionic liquids or gels are more durable. Other alternatives include solid-state hole transporters and cobalt-based systems.³ Iodide reduces the dye according to the following reactions:



The net products are regenerated dye and triiodide, which diffuses to the cathode where reduction occurs. This causes a positive charge to develop on the cathode and regenerates iodide according to the reaction



The diffusion rates of iodide and triiodide, solution viscosity, and vapor pressure mediate the efficiency of an electrolyte. Higher viscosity increases electrolyte concentration due to ionic and Van der Waals interactions, but it also inhibits electrolyte diffusion, so optimization of the HTL requires a balance of electrolyte concentration and diffusion.¹⁷ Vapor pressure is another double-edged sword because solutions with high vapor pressure have higher diffusion rates but those with low vapor pressure are more stable since they do not evaporate as much when subject to high temperatures. The prototypical electrolytes with low vapor pressures are ionic liquids, which nearly eliminate the need for hermetic sealing due to their low volatility at relevant temperature ranges. They may still utilize I⁻/I₃ as the mobile ions, but the solutions in which they are mobile have higher molecular weights than those of typical volatile solutions.¹⁸

1.7 Electron transport layer

The mesoporous metal oxide film in DSSCs provides a porous substrate with large surface area onto which dyes can adsorb, which is followed by electron injection into the film's conduction band and electron transport to the anode. Mesoporous TiO₂ films increase available surface area by about 1000-fold compared to nonporous films and were essential for Grätzel's breakthrough research in 1991.⁸ TiO₂ is an ideal electron transport layer (ETL) because it is nontoxic, stable, inexpensive, and widely available. Other metal oxide films commonly used include ZnO and SnO₂, but TiO₂ is the standard in current DSSC investigations. TiO₂ comes in

several crystal structures, and anatase is preferred for DSSCs due to its larger bandgap and higher conduction band edge energy, which result in larger V_{OC} in completed cells.³

TiO_2 is flexible in that it allows an array of preparatory and application procedures. Laboratories may opt for purchasing solid TiO_2 nanoparticles with determined sizes or prepare it themselves via hydrolysis of titanium precursors followed by hydrothermal growth and crystallization, which allows for increased control of crystal shapes and properties. The particles are solubilized to generate a paste, which is most commonly deposited onto electrodes by doctor blading or screen printing. Sintering the deposited film at around 450 °C forms electrical connections within TiO_2 and eliminates organic contaminants.³

State-of-the-art DSSCs employ additional deposition procedures of TiO_2 which include a blocking layer, a light scattering layer, and a thin overcoat. A blocking layer is an initial 50nm layer of dense, poreless TiO_2 deposited by spray pyrolysis, chemical bath deposition, or sputtering. This prevents contact and recombination between the conductive layer on the anode and the mobile redox electrolyte. Following is a 10 μ m light absorption layer, which is found in all DSSCs and serves to bind dye molecules to its surface. Next, a 3 μ m light-scattering layer of larger particles (~400 nm) is deposited with the intent of scattering light to increase incident light exposure. Finally, chemical bath deposition using $TiCl_4$ provides an ultrathin layer of TiO_2 , resulting in increased dye adsorption and enhanced injection efficiency due to lower energy of the TiO_2 conduction band.³

Undesirable recombination can occur when an electron moves from mesoporous semiconductor to oxidized redox electrolyte, from semiconductor to oxidized dye, and within the dye from excited state to resting state (Figure 7). The first type of recombination can be prevented by using spray pyrolysis to deposit a dense layer of TiO₂ onto the anode. The second form of recombination depends on electron density in the semiconductor, which is determined by light intensity. Recombination within the dye is rare in devices using Ru-based complexes due to the relative time scales of electron injection compared to excited state decay. Injection of an electron from the dye's excited state to the TiO₂ conduction band is a process that occurs on the order of femtoseconds, while the excited state lifetime is 20 – 60 ns. However, completed DSSCs have exhibited electron injection rates around 150 ps, a time interval long enough to allow kinetic competition of electron decay to adversely affect overall efficiency. Electron injection efficiency is given by

$$\varphi_{inj} = k_{inj} / (k_{inj} + k_1) \quad (7)$$

where k_{inj} is the rate constant for electron injection and k_1 is the rate constant for electron decay of the dye in its excited state. Efficient injection requires a k_{inj} value about 100 times greater than k_1 . Values for k_{inj} may be increased by engineering dyes to increase the difference between the dye's LUMO and TiO₂ conduction band.³

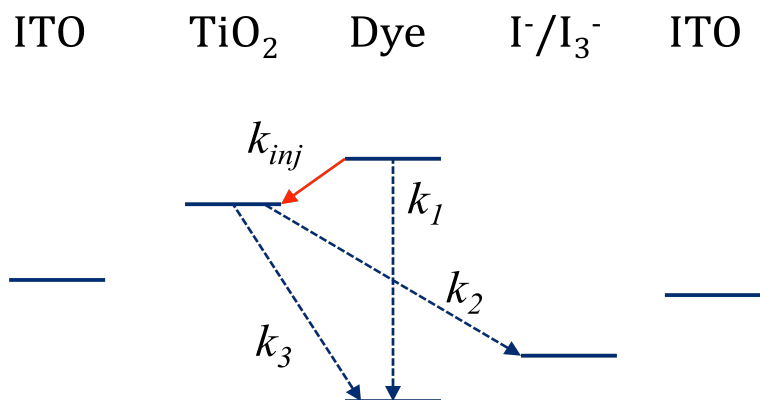


Figure 7. Energy diagram of DSSC showing recombination pathways (black) and injection rate (red). k_{inj} is the rate constant for electron injection from dye LUMO into TiO₂ conduction band; k_1 is the rate constant for electron decay within the dye from LUMO to HOMO; k_2 is rate constant for electron transfer from TiO₂ conduction band to redox electrolyte; k_3 is rate constant for electron transfer from TiO₂ conduction band to reduced dye's HOMO.

1.8 Experimental design

This laboratory thesis intends to construct functional DSSCs using biologically-derived dyes and to understand the merits and drawbacks of various procedures and dyes. The employed dyes are melanin, retinoic acid, and hemin (Figure 8). Melanin is a pigment found in many animals and is responsible for the process of pigmentation of human skin as a defense mechanism against carcinogenic solar UV-radiation. Melanin is not attributed with a molecular weight because it is thought to form cross-linked polymers of various sizes but neither the degree of polymerization nor the role of proteins are known, hence a solution containing melanin is in reality a mixture of distinct polymers.¹⁹ Retinoic acid is the oxidized form of retinaldehyde, which in human eyes is bound as a cofactor to rhodopsin in rod cells and allows us to perceive light.²⁰ Hemin is a iron-containing porphyrin that

is bound to the protein hemoglobin and functions to bind oxygen present in the lungs and release oxygen when it reaches muscles. Hemin is also present in myoglobin, which serves to store oxygen in muscles for times of high oxygen demand. Most importantly, hemin is structurally similar to chlorophyll, a protein that is ubiquitous in plants and serves to convert solar radiation to energy. Several research groups have implemented chlorophyll and chlorophyll derivatives in DSSCs with moderate success, which suggests that hemin may be similarly useful as a nontoxic and widespread sensitizer. The optical functionality of melanin, retinoic acid, and hemin inspires an investigation of their effectiveness as photoactive sensitizers in DSSCs.

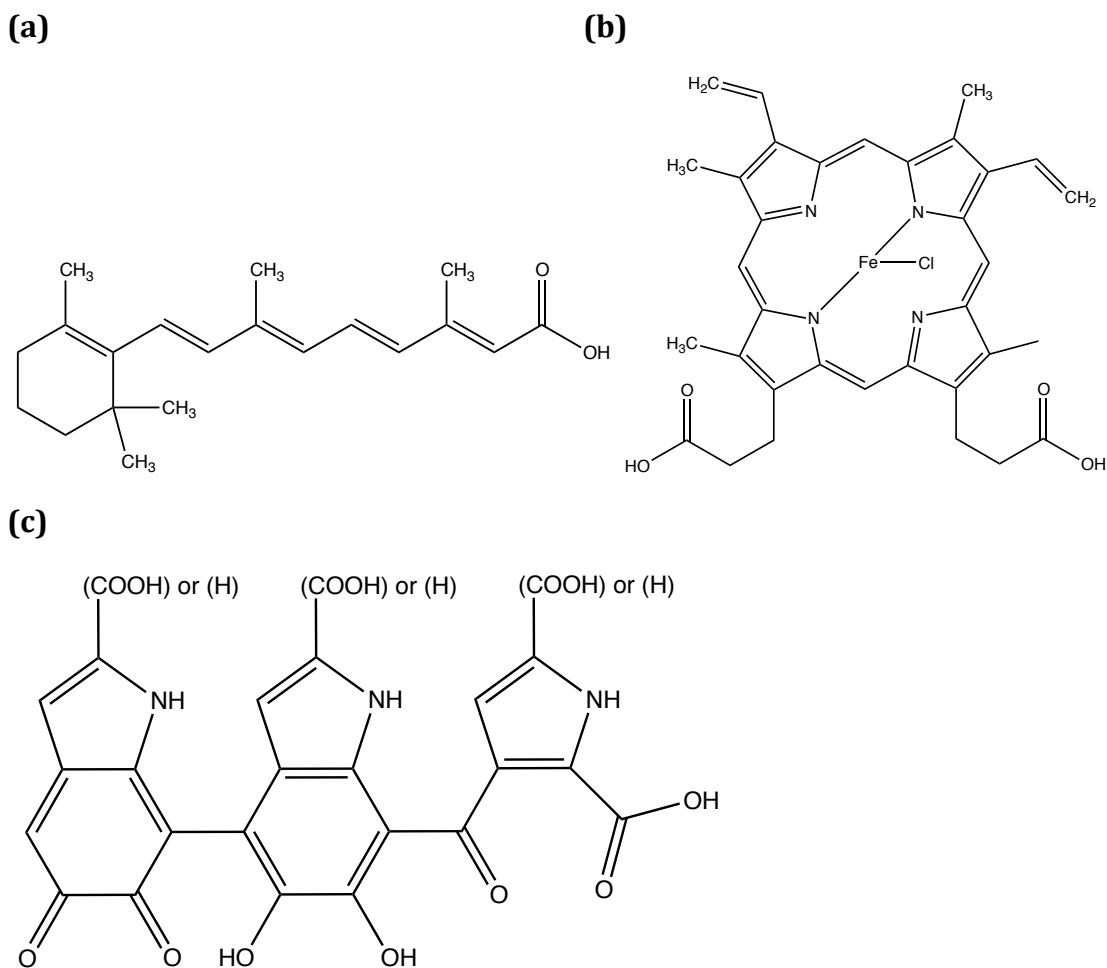


Figure 8. Structures of experimental dyes:(a) structure of all-trans-retinoic acid; (b) structure of hemin (ferriprotoporphyrin IX chloride); (c) partial structure of eumelanin, actual molecules are oligomers composed of cross-linked subunits of illustrated molecule.

Cell efficiency will be measured as a function of dye, temperature at which cells are hermetically sealed, and number of days elapsed since cell construction. Analysis of the last variable is longitudinal and therefore should not affect construction or analysis of the first two variables. The experimental approach entails optimizing the procedure to improve cell durability and efficiency, construction of several cells using different dyes and sealing temperatures, and repeated characterization of cell efficiency over a period of several days.

2. Experimental

2.1 Materials

TiO₂ nanopowder (diameter 21 nm, ≥99.5% trace metals basis) was purchased from Sigma-Aldrich. Melanin (CAS number 8049-97-6) was purchased from Sigma-Aldrich. Hemin (MW 651.95, from bovine, ≥95% purity) was purchased from Strem Chemicals. Retinoic acid (MW 300.44, ≥98% purity) was purchased from Sigma-Aldrich. N3 Ruthenizer 535 (MW 741.7) was purchased from Solaronix. H₂PtCl₆ catalyst (MW 517.90, ≥37.5% Pt basis) was purchased from Sigma-Aldrich. Meltonix 1170-25 sealing foil of thickness 25 μm was purchased from Solaronix.

2.2 Cell assembly

Solar cell construction entailed coating the anode with TiO₂ and immersing in photoactive dye, annealing the cathode with the anode using a sealing gasket, introducing I⁻/I₃⁻ electrolyte into the space between slides, and sealing the hole in the cathode to complete the hermetic seal.

Indium tin oxide (ITO)-coated glass slides with dimensions 2.5 cm x 2.5 cm x .5 cm served as both cathodes and anodes. Slides were cleaned by immersing in isopropanol, sonicating for 15 minutes, and drying, followed by UV-O₃ treatment for 15 minutes. A mixture of TiO₂ composed of 4.0 g TiO₂ nanopowder in 5 mL 200 proof ethanol and 5 mL nitric acid (1:500 dilution in distilled water) was prepared. 300 μL of this colloid was pipetted onto the ITO-coated side of a clean anode and

allowed to sit for 60 seconds. The anode was then spin-coated for 30 seconds at 1000 rpm using a Laurell model WS-400-6NPP spin coater. A cylindrical copper tube with diameter 1.1 cm was placed onto the TiO₂-coated slide and a nail file wrapped in a Kim-wipe was used to wipe off the surrounding TiO₂, leaving a circular film of wet TiO₂ on the anode. The TiO₂ layer was sintered onto slides by heating slides in a furnace at 500°C for 20 minutes.

Once anodes were cooled, they were immersed in glass slide stainers containing one of three dye solutions. The melanin solution was composed of 6 mg melanin in 50 mL ethanol (200 proof). The 0.606 mM retinoic acid solution was made in hexanes. The 0.476 mM hemin solution was made by solubilizing 15.53 mg of hemin in 400 µL of 50% NaOH_(aq) to hydroxylate the previously chlorinated metal ligand, and finally phosphate buffer solution (PBS, made in Milli-Q) was added to the hemin solution to achieve a total volume of 50mL. The 0.0906 mM N3 ruthenium solution was made in acetonitrile. Slides were left to soak in one of the above solutions for one to seven days (Figure 9).



Figure 9. Slides with TiO_2 after immersion in solutions of hemin, melanin, or retinoic acid for two days. Slides were removed from dye and rinsed with water followed by rinsing with ethanol and drying with compressed air.

Cathode slides were drilled through with 1mm diameter diamond tips with the drill moving from ITO-side to glass side. Slides were cleaned in the same manner as anodes, with sonication in isopropanol followed by UV- O_3 treatment. 2-3 drops of .005M H_2PtCl_6 catalyst in ethanol (190 proof) was dropped onto the ITO-coated side of cathodes, spread across the surface by tilting the slide, and allowed to dry in the fume hood for five minutes. The catalyst was annealed by heating slides in the furnace at 380°C for 20 minutes, leaving a pure Pt layer on the cathode.

To seal two slides together and make a cell, an anode was removed from dye solution, rinsed with distilled water, rinsed with ethanol (190 proof), and dried with a pressurized air nozzle. A hole punch with area slightly larger than that of the TiO_2 /dye circles was used to make a hole in the Meltonix sealing foil, and a square was cut around the circular hole to create a gasket with a border of approximately

2mm. This gasket was placed between anode and cathode by lining up the TiO₂/dye circle with the gasket hole with Pt-coated side of the cathode facing inward. Slides were heated on a hot plate at varying temperatures with cathode on the bottom until the gasket was visibly melted. Each cell was heated at a single temperature, but temperatures differed across cells to test the heat-dependent stability of the dye in use. The goal was to determine the highest sealing temperature a dye could withstand that would not deteriorate performance. After sealing, cells were allowed to cool to room temperature and then placed in a glass desiccator with cathode facing up. Two drops of 0.5M KI/0.05M I₂ in water-free ethylene glycol was dropped onto the hole in the cathode and the desiccator was sealed with a lid connected to a vacuum nozzle. A vacuum was applied to the cell, and proper sealing of the gasket was confirmed by evolution of bubbles out of the cathode. The vacuum was removed to allow the electrolyte to infiltrate the space between anode and cathode. Vacuum was applied and released up to three times until the TiO₂/dye circles were visibly covered in redox electrolyte solution. The hole in the cathode was sealed by covering the hole with a section of Meltonix, followed by a segment of microscope slide, and the sealing foil was melted with a soldering iron (CSI-Station1A). Cells were allowed to cool and were then characterized using linear sweep voltammetry.

2.3 Efficiency characterization

DSSCs were characterized using a model 1200B handheld potentiostat/bipotentiostat by CH Instruments. The computer program was set to

linear sweep voltammetry with the following parameter settings: initial E at -0.3V, final E at 0.5V, scan rate at 0.05 V/s, and sensitivity at 10^{-2} A/V. A tripod was placed onto a slide projector (Eclipse AI-2035), which was powered on and allowed to warm up for a minute. The working electrode was clipped to the cathode and the counter and reference electrodes were clipped to the anode. The cell was placed on the tripod with the interface between anode and cathode aligned with the horizontal plane of the tripod. A run was completed, saved, and analyzed in Microsoft Office Excel to derive I_{sc} , V_{oc} , FF, and efficiency. This process was performed on every solar cell immediately upon construction and repeated for several days afterward with the intent of collecting a more robust set of data for each cell that could potentially relate cell age to peak cell efficiency.

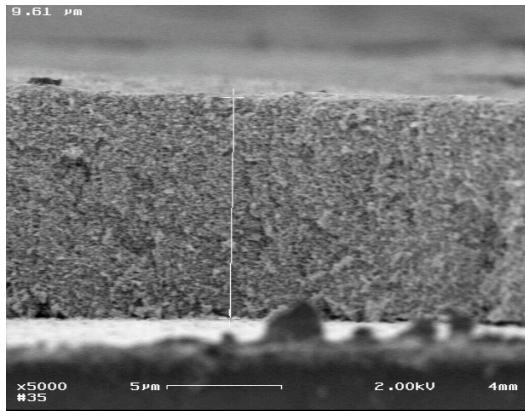
The absorbance spectra of dyes were determined using UV-visible spectroscopy. A Cary 300 Bio UV-Visible spectrophotometer was used in dual-beam mode to obtain spectra of each dye. All default settings were used except in the case of retinoic acid, for which the wavelength at which lamps switch over was changed from 350nm to 370 nm because peak absorption occurred at approximately 350nm and the change in lamps was distorting important data regarding peaks.

3. Results and discussion

3.1 Scanning electron microscopy

Analysis of TiO₂ film thickness using scanning electron microscopy (SEM) allowed optimization of our procedure in order to design films approximately 8 microns thick. We determined that a solution of 4 g TiO₂ in 5 mL 200 proof ethanol and 5 mL nitric acid (1:500 dilution in water) spin-coated for 30 seconds at 1000 rpm generates films of 6 to 9 μm thickness (Figures 10 and 11). Differences in film thicknesses across identical TiO₂ solutions and spin speeds are attributed to the length of time the paste was allowed to sit on the slide undisturbed before initiating spin-coating. Comparison of figures 10 and 11 demonstrates that pastes allowed to sit on slides for over 2 minutes before spin-coating generated considerably thicker films compared to slides that were spin-coated immediately after paste application. We determined that letting TiO₂ paste rest on slides for 60 seconds before spin-coating would generate relatively homogenous TiO₂ layers of 7-9 μm thickness. This is approaching the ideal TiO₂ film thickness of 10 μm that Grätzel used in his original DSSCs.

(a)



(b)

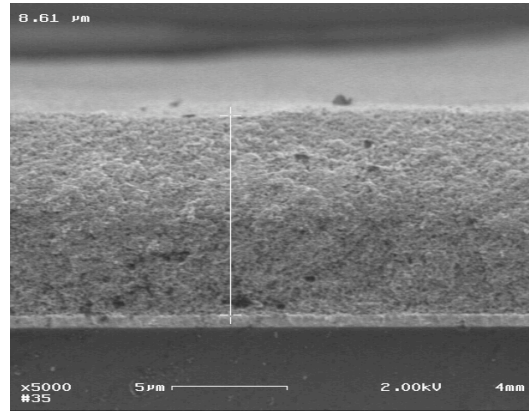
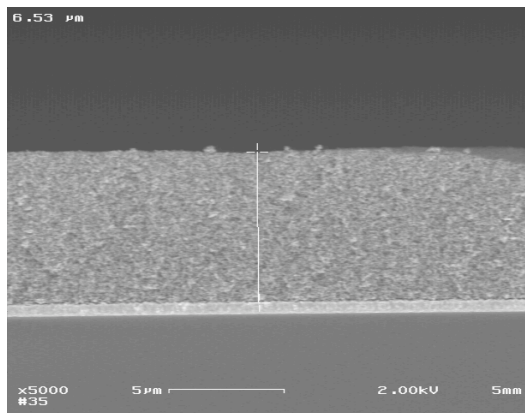


Figure 10. Cross-sectional images of TiO₂ layer on glass slide using scanning electron microscopy. TiO₂ solution was left on slide for over 2 minutes before spinning at 1000 rpm for 30 seconds, followed by sintering at 500°C for 20 minutes. Dark boundary at bottom is glass, gray layer being measured is TiO₂, and thin gray layer between the two is ITO layer. (a) TiO₂ layer is 9.61 μm thick; (b) TiO₂ layer at a different section of the slide is 8.61 μm thick.

(a)



(b)

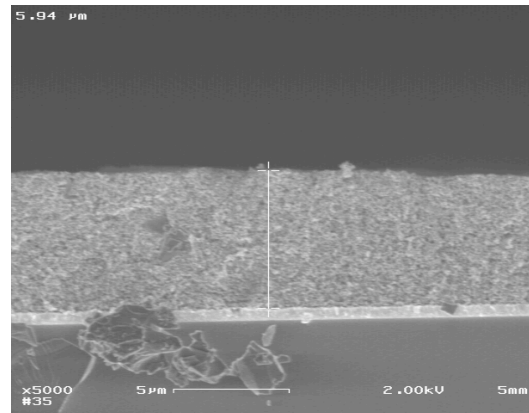


Figure 11. Cross-sectional images of TiO₂ layer on glass slide using scanning electron microscopy. Deposition of TiO₂ solution on slide was immediately followed by spin-coating at 1000 rpm for 30 seconds, followed by sintering at 500°C for 20 minutes. (a) TiO₂ layer is 6.53 μm thick; (b) TiO₂ layer at a different section of the slide is 5.94 μm thick.

It was concluded that film thickness varies across an individual slide depending on the location being examined. Based on the results indicating a correlation between film thickness and time of contact of TiO₂ with slide, we

hypothesized that pipetting the solution onto the center of the slide and letting it spread was allowing particles in the center to adhere to the slide more effectively than particles that achieved contact with the slide via gravitational forces and/or the centrifugal acceleration of the spin coater. However, SEM analysis did not reveal a trend of thicker films in the middle of a slide compared to the outer edges of the same slide. We nevertheless addressed this potential procedural problem by pipetting TiO₂ paste onto the entire surface of the slide before spin-coating in order to allow equal adhesion of nanoparticles to all areas of the slide. Further studies of TiO₂ interactions with ITO glass slides on a molecular level would enhance an understanding of why time of contact is a key variable in determining film thickness and what causes variability of film thickness across a single slide.

3.2 UV-visible spectroscopy

Spectroscopic analysis yielded absorbance spectra for the three dyes and a molar extinction coefficient of 48,326 M⁻¹cm⁻¹ for retinoic acid and 47,240 M⁻¹cm⁻¹ for hemin (Figure 12). Melanin does not have a molecular weight due to the variability in its polymeric structure, so calculation of its molar extinction coefficient is not feasible. In addition, melanin was not fully soluble in the solvents acetonitrile and tert-butanol. This resulted in melanin particles scattering incident light instead of absorbing light, which explains why its absorption spectrum has no defined peaks. Successful solvation of melanin in a different solvent should yield a more accurate spectrum with clear peaks. Assays of retinoic acid using solutions of

23.03 μ M and 2.879 μ M indicated maximum absorbance (A_{\max}) of 1.202 at 352nm and A_{\max} of 0.128 at 351 nm, respectively. Hemin solutions of molarities 14.31 μ M and 7.154 μ M indicated A_{\max} of 0.676 at 385nm and A_{\max} of 0.318 at 386nm, respectively. These absorbance values were used with Beer's law to calculate the molar absorption coefficients of retinoic acid and hemin, and then averaged to obtain final values.

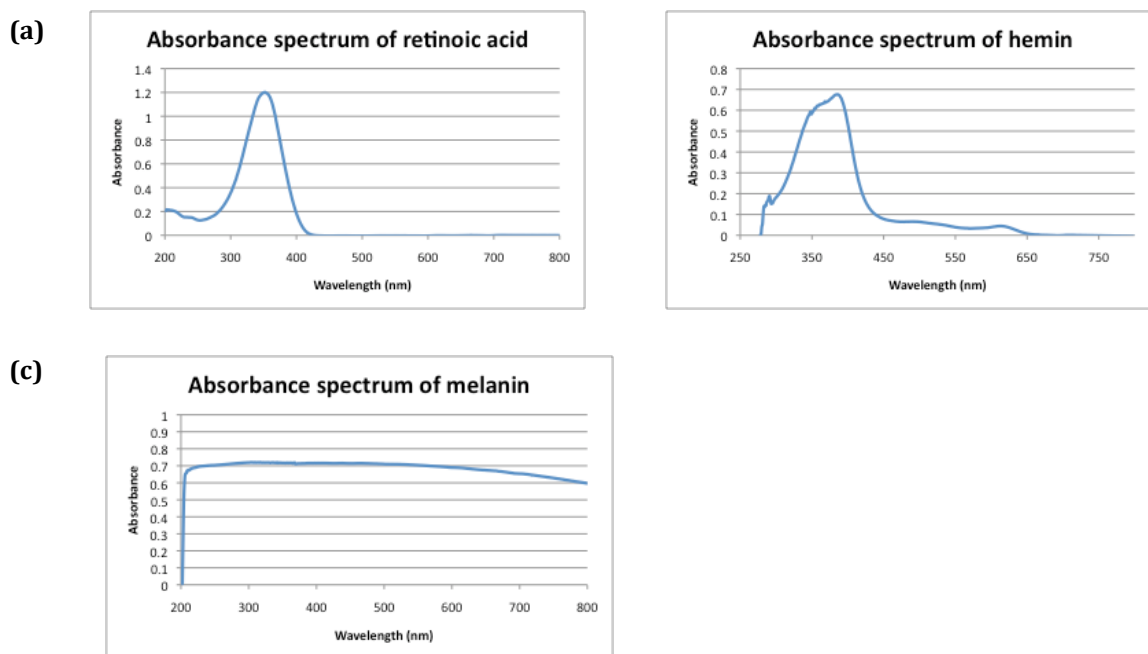


Figure 12. UV-visible absorbance spectrum of retinoic acid and melanin. (a) 23.03 μ M retinoic acid in hexane has A_{352} of 1.202; (b) 0.014 μ M hemin in PBS has A_{385} of 0.676; (c) Melanin (6.17mg in 25 mL tert-butanol/25 mL acetonitrile) has A_{304} of 0.7206.

3.3 Voltammetry

Linear sweep voltammetry yields data regarding voltage applied to a solar cell and the resulting current, which permits calculation of a DSSC's maximum power output and overall efficiency by using equation 2. J_{SC} takes into account the surface area of the cell, which is 1cm^2 for this project. A power meter reported that P_{in} , the incident power of our light projector, was 0.07W , allowing us to calculate overall conversion efficiency according to equation 2:

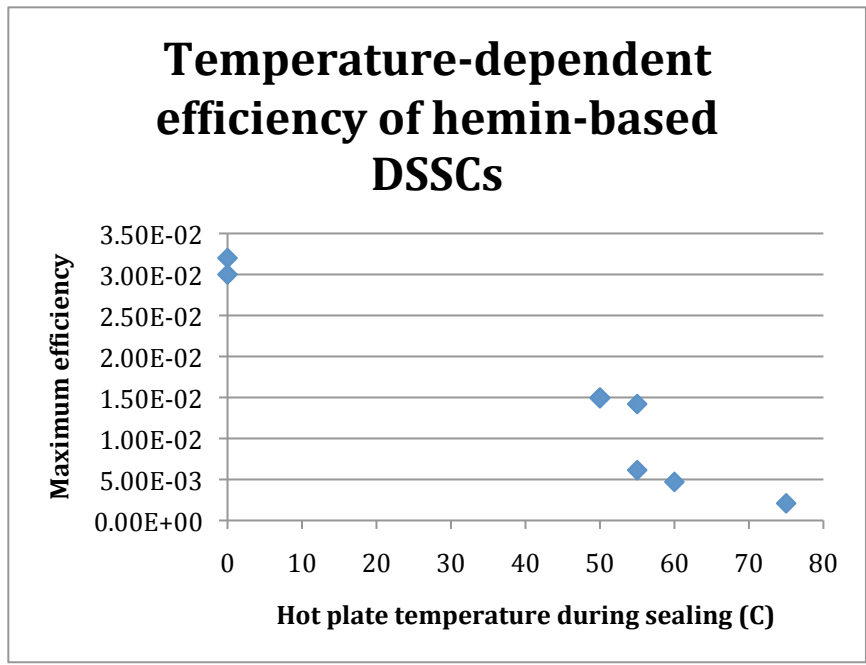
$$\eta = \frac{J_{SC} V_{OC} FF}{P_{in}} = \frac{P_{max}}{0.07} * 100\%$$

Voltammetry assays were performed on each cell for consecutive days with the hope of revealing patterns regarding maximum efficiency as a function of days after construction. However, cells were not reproducible with respect to peak efficiency versus time; some cells performed best immediately upon construction while others had peak efficiencies as long as eight days after construction. Improvement of cell efficiency over time could be a function of relaxation of dye molecules or completion of chelation of dye molecules to TiO_2 layer. Decrease of cell efficiency over time is likely a result of degradation of the dyes, which may be caused by small amounts of air trapped in the cell chamber oxidizing the biological dyes. The liquid redox electrolyte could also be involved in undesirable oxidations of the sensitizers. The overall variability in timing of peak efficiency may also be attributable to a number of uncontrolled factors such as temperature and humidity of the laboratory and the amount of time cells were exposed to air between each

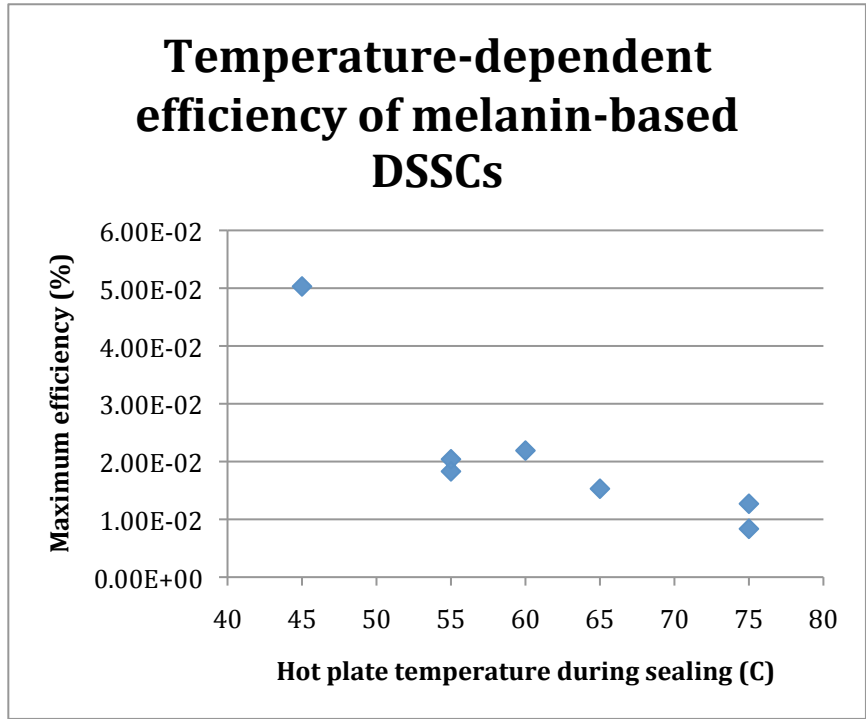
step of the procedure. The latter variable would account for increased oxidation of dyes within cells that remained exposed to room air between procedural steps. This could be addressed by constructing cells in an inert nitrogen atmosphere, which would prevent oxidation of dyes by oxygen in the air. Improved control of all potential variables would likely improve the reproducibility of peak efficiencies of cells in relation to time after construction. Taking measurements over a longer period of time is also necessary if such cells are to be marketable because economically viable PVs must offer a lifetime of several years.

The second variable tested in relation to cell performance was temperature at which the hot plate was set during the annealing of cathode to anode. This is an important step in the procedure because heat is required to melt the gasket and ensure a hermetic seal. Cells sealed at 45°C consistently leaked iodine, while those sealed at 50°C or higher were reproducibly airtight. On the other hand, all dyes in this project are biologically-based, which suggests that too high of a temperature will damage the molecules. This hypothesis was proven correct in the case of hemin and melanin (Figure 13). Hemin cells constructed without any sealing process performed impressively upon construction, although they were unstable over time due to constant leaking of liquid electrolyte. However, hemin cells sealed on the hot plate consistently performed worse than both melanin and retinoic acid. These results indicate that hemin is a functional sensitizer for DSSCs but it cannot withstand temperatures of even 45°C. Melanin demonstrates similar tendencies toward higher efficiencies when lower sealing temperatures are employed, but the correlation is not as robust. Melanin cells sealed at any temperature performed

better than hemin cells sealed at any temperature, with the exception of one poorly performing melanin cell. Based on the human body's normal temperature of 37°C, it is probable that a sealing procedure that takes place at 37°C or lower would not cause major damage to hemin molecules and would thus produce cells with efficiencies comparable to those of cells containing melanin and retinoic acid. Growth of the solar cell industry may promote demand for innovative chemical engineering that will allow hermetic sealing at lower temperatures.



(a)



(b)

Figure 13. Scatter plot of temperature during gasket sealing vs. maximum efficiency of hemin-based DSSCs. (a) The plot for hemin demonstrates a strong correlation between lower temperatures and higher efficiencies; (b) The plot for melanin demonstrates a moderate correlation between lower temperatures and higher efficiencies.

Quantification of solar cell performance was achieved by attributing each cell with the value of the maximum efficiency it yielded over the course of several days (Table 1, supplemental data). Calculation of an average of these maximum efficiencies resulted in one efficiency value per dye: 0.059% for retinoic acid, 0.023% for melanin, and 0.015% for hemin. Figure 14 presents I-V curves for the most efficient cells constructed for each of the three dyes. Hemin cells tended to produce the highest V_{OC} and FF values while retinoic acid produced the highest overall efficiencies.

Although these efficiency values are much lower than those of marketable PVs, it is important to consider whether it is the procedure or the choice of dyes that causes the low efficiencies. Cells constructed with N3, a ruthenium-based sensitizer, produced maximum efficiencies with an average of 1.46%. This is much lower than the typical N3 efficiencies, which yield efficiencies as high as 11% in conjunction with IL electrolytes.¹² Ruthenium cells made for this project had efficiencies lower by a factor of about seven compared to those produced for published papers, so it is reasonable to presume that DSSCs constructed in more specialized labs with enhanced experimental procedures would yield efficiencies about seven times higher than those calculated in this project. Another method of evaluating prototype cell efficiencies is to compare them to the ruthenium cells made in the same lab. Calculation of the ratios of average maximum efficiency of ruthenium cells to average maximum efficiency of biological cells suggests that ruthenium cells yield efficiencies 25 times that of retinoic acid cells, 63 times that of melanin cells, and 97 times that of hemin cells.

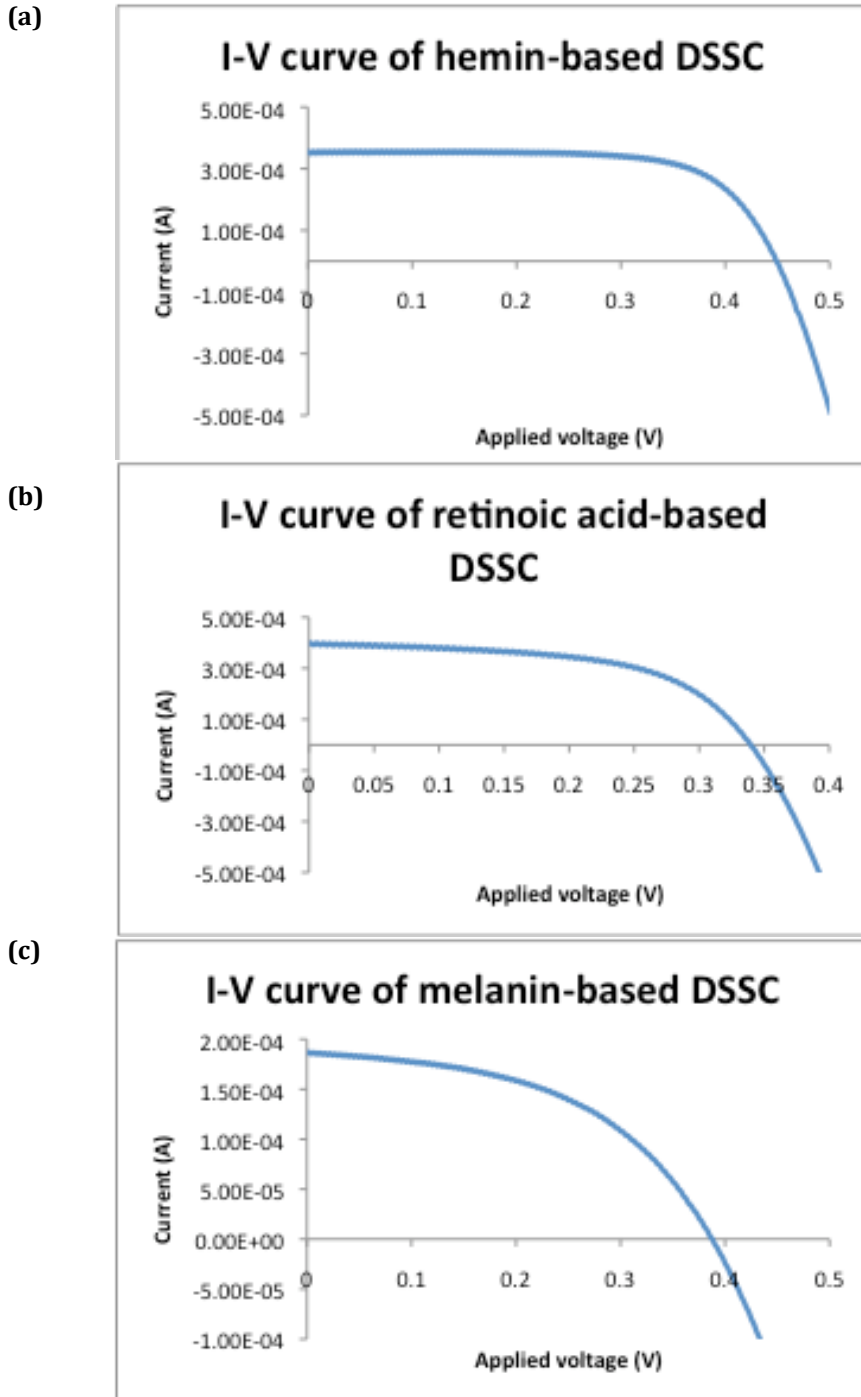


Figure 14. I-V curves of highest performing DSSCs constructed using hemin, retinoic acid, and melanin as dyes. (a) The highest performing hemin-based cell yielded efficiency of 0.032%, J_{sc} of 71.2 $\mu\text{A}/\text{cm}^2$, V_{oc} of 0.449V, P_{max} of 0.112mW, and FF of 0.7; (b) The highest performing retinoic acid-based cell yielded efficiency of 0.109%, J_{sc} of 398 $\mu\text{A}/\text{cm}^2$, V_{oc} of 0.339V, P_{max} of 0.0766mW, and FF of 0.57; (c) The highest performing melanin-based cell yielded efficiency of 0.0503%, J_{sc} of 186 $\mu\text{A}/\text{cm}^2$, V_{oc} of 0.387V, P_{max} of 0.0352 mW, and FF of 0.49.

Future paths for this project may take advantage of these dyes' specific strengths by making cells with a combination of hemin and retinoic acid. Hemin has maximum absorption peaks at 385nm and 613nm while retinoic acid has maximum absorption at 352nm, so combining these dyes would increase the spectrum across which a cell responds most effectively. One complication of this approach is the difference in polarities of the sensitizers: retinoic acid is nonpolar and dissolves well in hexane, while hemin is polar and very soluble in water. When considering how to introduce both dyes into a cell, a sequential deposition of one sensitizer followed by the other may be preferable if solubilizing both compounds in one solution is not feasible. Melanin may also be a good candidate for cells with multiple dyes, but an appropriate solvent must be determined in order to achieve a satisfactory absorption spectrum and to improve adsorption of dye molecules to TiO₂ during the soaking period. Finally, the temperature-induced decomposition of hemin must be addressed if hemin cells are to be sealed using the same procedure.

4. Conclusions

This project demonstrates that hemin, retinoic acid, and melanin can be used as photoactive dyes to construct functional DSSCs. These compounds are economically and environmentally superior to ruthenium-based sensitizers in that they are nontoxic and widely available due to their biological origins. SEM analysis enhanced the procedure for making TiO₂ films, which improves overall efficiency of cells. UV-visible spectroscopy revealed maximum absorption wavelengths for hemin and retinoic acid, which allowed calculation of molar absorption efficiencies. Extensive work on laboratory setup and acquisition of equipment will also aid the continuation and reputability of this project.

These experiments inspire several questions regarding improvement of biologically-based DSSCs. Cells made with hemin or melanin showed improved efficiencies with the use of lower sealing temperatures, which is understandable since both compounds are primarily found in animals that do not reach temperatures of 50°C. By the same token, these dyes may have undergone oxidative damage during all the construction processes, which took place in room air instead of in an inert nitrogen atmosphere. DSSCs made with a combination of dyes will likely improve the absorption spectra of cells, which would increase overall efficiencies. These photoactive biological dyes offer many opportunities for the improvement of environmentally conscious DSSCs.

5. Acknowledgements

I thank Professor Johal for his guidance over the years and during my preparation of this thesis. I would also like to give thanks to Charles Taylor and Willie Crane for their help over the summer and to the physics department for allowing me to use their scanning electron microscope. Kudos to Robo Bodor for being a patient, practical, and goofy lab partner who kept me sane all summer. Funding for this project was provided by the Pomona College Chemistry Department.

6. Supplemental data

Dye	Maximum efficiency over several assays (%)	Sealing temperature (°C)/time slide soaked in dye solution (days)
Retinoic acid	0.0189	75/2
	0.0467	75/2
	0.109	75/1
	0.0817	65/1
	0.0706	55/1
	0.0414	55/2
	0.0594	45/2
	0.0427	50/3
Melanin	0.00836	75/2
	0.0219	60/2
	0.0127	75/1
	0.0153	65/1
	0.0204	55/1
	0.0183	55/2
	0.0503	45/2
	0.0351	50/3
Hemin	0.00209	75/2
	0.00470	60/2
	0.0320	0/1
	0.0300	0/1
	0.0150	50/3
	0.0149	50/4
	0.0142	55/4
	0.00614	55/4
Ruthenium	1.01	*/1
	1.91	*/2

Table 1. Tabulation of maximum efficiencies for each cell. Included is information on temperature of hot plate during sealing and number of days each anode slide was soaked in dye solution.

* Ruthenium cells were sealed using a soldering iron at an unknown temperature

7. References

- ¹ Rogner, H.; Zhou, D., Bradley, R.; Crabbé, P.; Edenhofer, O.; Hare, B., Kuijpers, L.; Yamaguchi M.: Introduction. In: *Climate Change 2007: Mitigation. Contribution of Working Group III to the Fourth Assessment Report of the Intergovernmental Panel on Climate Change*; Metz, B.; Davidson, O.R.; Bosch, P.R.,; Dave, R.; Meyer, L.A., Eds.; Cambridge University Press: Cambridge, United Kingdom and New York, NY, **2007**.
- ² Grätzel, M. Photovoltaic and photoelectrochemical conversion of solar energy. *Phil. Trans. R. Soc. A*. **2007**, *365*, 993-1005.
- ³ Hagfeldt, A.; Boschloo, G.; Sun, L.; Kloo, L.; Pettersson, H. Dye-sensitized solar cells. *Chem. Rev.* **2010**, *110*, 6595-6663.
- ⁴ Darling, D. I-V curve (of a photovoltaic device).
http://www.daviddarling.info/encyclopedia/I/AE_I-V_curve.html (accessed Nov 9, 2011).
- ⁵ Rohde, R.A. Solar Radiation Spectrum.
http://www.globalwarmingart.com/wiki/File:Solar_Spectrum_png (accessed Nov 9, 2011).
- ⁶ Guo, X.; Luo, Y.; Zhang, Y.; Huang, X.; Li, D.; Meng, Q. Study on the effect of measuring methods on incident photon-to-electron conversion efficiency of dye-sensitized solar cells by home-made setup. *Rev. Sci. Instrum.* **2010**, *81*, 1-9.

⁷ Perlin, J. *From Space to Earth: The Story of Solar Electricity*; Routledge: 1999.

⁸ Grätzel, M. A low-cost, high-efficiency solar cell based on dye-sensitized colloidal TiO₂ films. *Nature*. **1991**, *353*, 737-740.

⁹ Schoonman, J. Nano-structured materials for the conversion of sustainable energy. *Nanostructured and advanced materials for applications in sensor, optoelectronic and photovoltaic technology*. **2005**, 271-280.

¹⁰ Grätzel, M. Solar energy conversion by dye-sensitized photovoltaic cells. *Inorg. Chem*. **2005**, *44*, 6841-6851.

¹¹ Sündstrom, V.; Kathiravan, A.; Yartsev, A.; Infahsaen, Y. Interfacial electron transfer in whole functional dye-sensitized solar cell.
<http://www.chemphys.lu.se/research/projects/wholedssc> (accessed Nov 9, 2011).

¹² Grätzel, M. Conversion of sunlight to electric power by nanocrystalline dye-sensitized solar cells. *J. Photoch. Photobio. A*. **2004**, *164*, 3-14.

¹⁴ Desilvestro, H.; Hebting, Y. Ruthenium-based dyes for dye solar cells.
<http://www.sigmaaldrich.com/materials-science/organic-electronics/dye-solar-cells.html> (accessed Nov 9 2011).

¹⁵ Ruthenium (Ru) – Chemical properties, health and environmental effects.
<http://www.lenntech.com/periodic/elements/ru.htm> (accessed May 6, 2011).

¹⁶ Dierks, S. Ruthenium Material Safety Data Sheet.

<http://www.espimetals.com/index.php/online-catalog/237-ruthenium> (accessed May 6, 2011).

¹⁷ Hao, F.; Lin, H.; Zhang, J. Li, J. Balance between the physical diffusion and the exchange reaction on binary ionic liquid electrolyte for dye-sensitized solar cells. *Journal of Power Sources*. **2011**, *196*, 1645-1650.

¹⁸ Hallett, J.; Welton, T. Room-temperature ionic liquids: solvents for synthesis and catalysis. *Chem. Rev.* **2011**, *111*, 3508-3576.

¹⁹ Jacques, S. Optical Absorption of Melanin.

<http://omlc.ogi.edu/spectra/melanin/index.html> (accessed Nov 19, 2011).

²⁰ Saam, J.; Tajkhorshid, E.; Hayashi, S.; Schulten, K. Molecular dynamics investigation of primary photoinduced events in the activation of rhodopsin. *Biophysical journal*. **2002**, *83*, 3097-3112.